Supplementary Information

Water-based Solar Cell over 10% efficiency: Designing Soft Nanoparticles for improved Processability

Alexandre Holmes[1], Hugo Laval[2], Michele Guizzardi[3, 4], Valentina Maruzzo[1, 5], Giulia Folpini[3, 4], Nadia Barbero[5], Elise Deniau[1, 6], Marc Schmutz[7], Sylvie Blanc[1], Annamaria Petrozza[3, 4], Giuseppe Maria Paterno[3, 4], Guillaume Wantz[2], Sylvain Chambon[2]*, Christine Lartigau-Dagron[1]*, Antoine Bousquet[1]*

1. Universite de Pau et Pays de l'Adour, E2S UPPA, CNRS, IPREM, Pau, France
2. Université de Bordeaux, CNRS, Bordeaux INP, IMS, UMR 5218, F-33400 Talence, France
3. Department of Physics, Politecnico di Milano, Milano 20133, Italy
4. Center for Nano Science and Technology@PoliMi, Istituto Italiano di Tecnologia, Milano 20134, Italy
5. University of Torino, Department of Chemistry, NIS Interdepartmental Centre and INSTM Reference Centre, Via Quarello 15a, 10135, Turin, Italy
6. Université du Mans, Institut des Molécules et Matériaux du Mans, UMR CNRS 6283, Le Mans, France
7. Université de Strasbourg, PLAMICS, CNRS, Institut Charles Sadron-UPR22, Strasbourg, France

Experimental section

Materials

Tetrahydrofuran (THF, >), chloroform (> 99%), sodium dodecyl sulfate (SDS), ethanolamine (> 99.5%), ethanol (> 99.8%), and zinc acetate dihydrate were purchased from Sigma Aldrich. MoO_3 powder was purchased from NEYCO. Milli-Q water was obtained from a Synergy® UV Millipore system (18.2 MΩ). PTQ10 (M_w = 110 kg.mol^{-1}) and Y6 were purchased from 1-Material and were used without further purification.

Nanoparticle synthesis

Nanoprecipitation technique: First, 6.8 mg of PTQ10 and 8.2 mg of Y6 were solubilized in 30 mL of THF at 80°C for 3 hours. In 200 mL of Milli-Q water, 600 mg of SDS was solubilized. The organic phase was then quickly injected into the aqueous phase under vigorous stirring (750 RPM). THF was removed using a nitrogen flow at 65°C for 2 hours. *Miniemulsion technique*: For the organic phase, a solution of PTQ10:Y6 (wt% of 1:1.2) in chloroform (25 mg.ml^{-1}) was stirred for 2 h at 65°C in a nitrogen-filled glovebox. The aqueous phase was obtained by dissolving 5 mg.ml^{-1} SDS in deionized water and stirring for 30 min at RT. A macroemulsion was obtained by adding the organic phase into the aqueous phase

(1:5 volume ratio) and stirring for 1 h at 40°C (1000 rpm). The miniemulsion was formed by sonicating the macroemulsion using a BRANSON Digital Sonifier 450 in an ice-water bath for 2 min at 17% of the maximum power. Chloroform evaporation was performed by stirring the miniemulsion for 3 h at 65°C, resulting in PTQ10:Y6 dispersions.

Nanoparticle characterization

Dynamic light scattering (DLS) was performed on a Nano-ZS Zetasizer (Model ZEN3600 Malvern Instruments) operating at an angle of 173° (hydrodynamic diameters Dh and polydispersity (PDI)). Nano-ZS is equipped with a He-Ne 4.0 mW power laser operating at a wavelength of 633 nm. The particles were dispersed in Milli-Q water at a concentration of 0.05 $g.L^{-1}$. The data were calculated using cumulant analysis.

UV–visible absorption spectra of P3HT:$PC_{61}BM$ nanoparticles were recorded on a Shimadzu UV-2450PC spectrophotometer with a path of 1 cm in a quartz cell. Emission spectroscopy (photoluminescence) was conducted using a 1 cm fluorescence quartz optical cell. All dispersions were concentrated to show an absorbance of 0.1 at the excitation wavelength used for PTQ10 or Y6 fluorescence. In the case of the PTQ10 fluorescence study, the corrected steady-state luminescence spectra were measured with excitation at 560 nm and scanning between 600 and 830 nm at 2 nm resolution using a photon counting Edinburgh FLS920 fluorescence spectrometer equipped with a xenon lamp. For the Y6 fluorescence study, luminescence spectra were measured with excitation at 812 nm and scanning between 830 and 950 nm at 1 nm resolution using a Fluorolog 3 TCSPC Horiba Jobin Yvon fluorescence spectrometer equipped with a 450-Watt illuminator (model FL-1039A) and an R13456 photomultiplier (Horiba Instruments Inc.). Calculation of the charge transfer efficiency n_Q was done by comparing the integrated emission spectra of the composite nanoparticles to that of pristine materials, over all the range of measured emission.

Contact angle

Contact angles were measured using a GBX contact angle meter, DGD Fast/60. For the film preparation, PTQ10 and Y6 were first solubilized in chloroform at 10 mg/mL at 60°C for 3 hours. The solutions were cooled down and then spin coated on glass substrates at 1000 RPM for 60 seconds (acceleration of 3 seconds). Finally, the substrates were annealed for 10 minutes at 100°C under a nitrogen atmosphere.

Cryogenic Transmission Electron Microscopy

A drop of 5 µL of the solutions at a concentration of 10 mg/mL was applied to a copper grid covered with a carbon film made hydrophilic using an ELMO glow discharge device (Cordouan Technologies, France). The grid was placed in a homemade vitrification apparatus at 22°C and 80% relative humidity

before plunging into liquid ethane maintained at -190°C by liquid nitrogen. The grid was mounted on a cryo-holder (Gatan 626, USA) and observed with a Tecnai G2 microscope (FEI, The Netherlands) at 200 kV. Images were acquired using an Eagle slow scan CCD camera (FEI).

Transient Absorption Spectroscopy (TAS)

A regeneratively Ti:sapphire laser emitting 100 fs pulses at 800 nm with a repetition rate of 1 kHz was used to generate pump and probe beams. A broadband white light probe in the visible and near infrared region was generated by focusing the output of a home-built Noncollinear Optical Parametric Amplifier (NOPA) tuned at 1240 nm into a 4 mm thick YAG crystal. To excite the sample, we used the fundamental beam at 800 nm or tuned it by using another NOPA fed by the second harmonic of the fundamental beam, and we centered it at approximately 550 nm with a bandwidth of 10 nm. For TAS at long delays, a YB:KGW amplified femtosecond laser system (Light Conversion Pharos, 1032 nm, 2 kHz) was used to produce a visible probe by filamentation in a 2 mm sapphire window. The pump consisted of a second harmonic (532 nm) Nd:YVO4 nanosecond diode laser (Innolas Picolo, 1064 nm, 900 ps, 1 kHz), synchronized with the probe with a variable delay using a digital delay generator.

Calorimetry

TGA was performed on a TGA 2, Mettler Toledo STAR® system with a heating rate of 10°C.min^{-1} under a nitrogen atmosphere. The PTQ10:Y6 nanoparticle dispersions were first freeze-dried using a CRIOS-80 Cryotec to remove the aqueous dispersant. The nanoparticles were then recovered in an alumina crucible and characterized by TGA. DSC measurements were performed on a DSC 3, Mettler Toledo STAR® system under a nitrogen atmosphere. For each sample, the temperature was increased from 25°C to 200°C at 10°C.min^{-1} and then cooled to 25°C following the same ramp. For the blend PTQ10:Y6 cast from chloroform, a solution of 15 mg.mL^{-1} was prepared, dropped in the crucible and evaporated several times to accumulate enough material.

Dispersion purification and concentration

To eliminate the excess surfactant and concentrate the inks at 60 mg.ml^{-1}, centrifugal steps were carried out by using an Amicon Ultra15 centrifuge filter (cutoff 100 kg.mol^{-1}) and a Beckman Coulter Avanti J-30I centrifuge. For nanoprecipitation-based dispersions, a first batch of centrifugation at 30°C, 3000 RPM and 6 minutes was used to reduce the volume from 200 mL to 12 mL. Then, four centrifugation cycles were performed at 2500 rpm for 6 min. For miniemulsion-based dispersions, five centrifugation cycles were carried out at 2200 rpm for 9 min. In both cases, the retentate was raised to 15 mL with deionized water between each step.

Atomic Force Microscopy

Atomic force microscopy (AFM) was performed on a Multimode®8 Atomic Force Microscope from Bruker using the PeakForce Quantitative NanoMechanics QNM mode in air. Characterization was performed directly on the active layer deposited under the same conditions as solar cells.

Device fabrication and characterization

OPV devices were fabricated using an inverted architecture glass/ITO/ZnO/active layer/MoO_3/Ag. ITO covered glasses were purchased from VisionTek with a sheet resistance of 10 Ω/sq. They were cleaned by sequential ultrasonic treatments: diluted Hellmanex™ III (2%), three successive steps of deionized water and a final step of isopropanol. For the electron transport layer, a ZnO precursor solution was prepared by mixing zinc acetate dihydrate (166 mg) and ethanolamine (45 µL) with absolute ethanol (5 mL). The solution was then stirred at 55°C in air for 30 min and left at room temperature under continuous stirring until final use. Substrates were dried and cleaned by UV-ozone for 15 min, and then the ZnO precursor solution was spin-coated to form thin films (3000 RPM, 60 s). The substrates were thermally annealed in air at 180°C for 45 min and treated with UV-ozone for 20 min before deposition of the water-based dispersions. The active layers were obtained by spin coating the nanoparticle dispersion (60 mg/mL) with a rotation speed of 2000 RPM. Annealing the film was performed in a nitrogen-filled glovebox. Afterwards, thermal evaporation under high vacuum (P = 10^{-6} mbar) was used to deposit a hole transport layer of MoO_3 (7 nm thick with a rate of 0.8 Å.s^{-1}) and a silver electrode (80 nm thick with a rate of 2 Å.s^{-1}). The area of OPV devices was defined as 10.5 mm^2 using a shadow mask during evaporation of the top electrode. OPV devices were characterized with a xenon lamp solar simulator (Newport LCS 100) under AM 1.5G conditions and with the light intensity set at 100 mW.cm^{-2} using a calibrated silicon reference cell (ABET Technologies, model 15150 with KG5 window). The J-V curves were recorded in the dark and in light using a Keithley 2400 SMU, and parameters were directly extracted via a LabVIEW program. For devices prepared from chloroform, the overall procedure is the same, except for the active layer. Fifty microliters of a PTQ10:Y6 solution in chloroform (ratio 1:1.2, 12 mg/mL) was spin coated onto a glass/ITO/ZnO substrate at 1000 RPM and annealed at 100°C for 10 minutes. External quantum efficiency (EQE) measurements were carried out using a PVE300 Photovoltaic EQE from Bentham Co. EQE was performed in ambient atmosphere, and all OPV devices were encapsulated.

Supplementary figures:

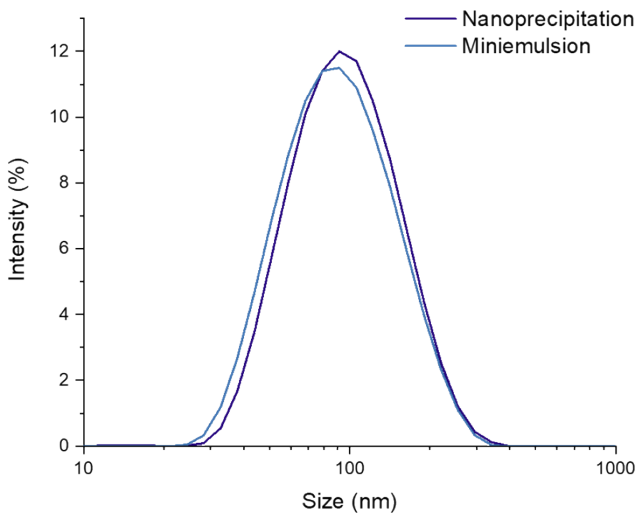

Figure S1. Size distribution of PTQ10:Y6 NPs prepared by nanoprecipitation and miniemulsion respectively. Data extracted from Dynamic Light Scaterring measurements (DLS). All dispersions are stabilised by SDS.

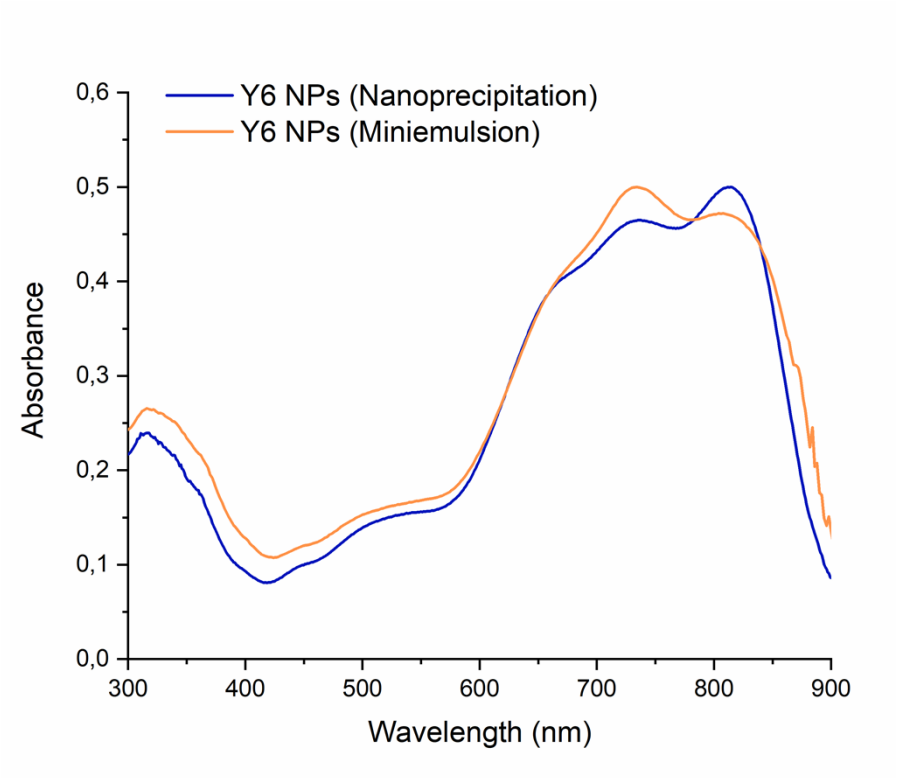

Figure S2. UV-Visible absorption spectra of pristine Y6 nanoparticles prepared by nanoprecipitation or miniemulsion.

<u>Supplementary note 1:</u>

To further investigate the change in Y6 structuration, pristine Y6 nanoparticles of the same size were prepared by both techniques and characterised by spectrophotometry Figure S2. Regardless the technique, no shift of the absorption bands was observed and attributed to the formation of similar Y6 domain size. However, a strong difference in ratio between both bands (814 and 730 nm) was identified, the main absorption band being at 730 nm for miniemulsion-based nanoparticles. Kroh *et al.* proposed that these two bands are attributed to different aggregations of Y6 molecules, called type I and II, identified here at 814 nm and 730 nm, respectively.[1] Type I promotes the overlapping of central core (C) and terminal moieties (T) of Y6 molecules in CT-CT or CC-TT aggregates, resulting in reduced energy levels (1.52 eV, absorption at 815 nm).[2] Type II promotes the formation to CT or TT aggregates (1.62 eV, absorption at 765 nm).

Although less noticeable in the case of composite PTQ10:Y6 nanoparticles (Figure 2a), the study of Y6 pristine nanoparticles appeared to show that nanoprecipitation resulted in the formation of type I aggregates (maximum absorption at 814 nm). In comparison, miniemulsion promoted the formation of type II aggregates (increased absorbance at 745 nm for composite PTQ10:Y6 nanoparticles). The formation of type I aggregates (especially CC-TT configuration) was proved to present the highest electronic couplings and transport rates for electrons, holes, and excitons.[2] Once integrated in solar cells, this might result in a reduced energetic disorder and optimized performances.[1,3]

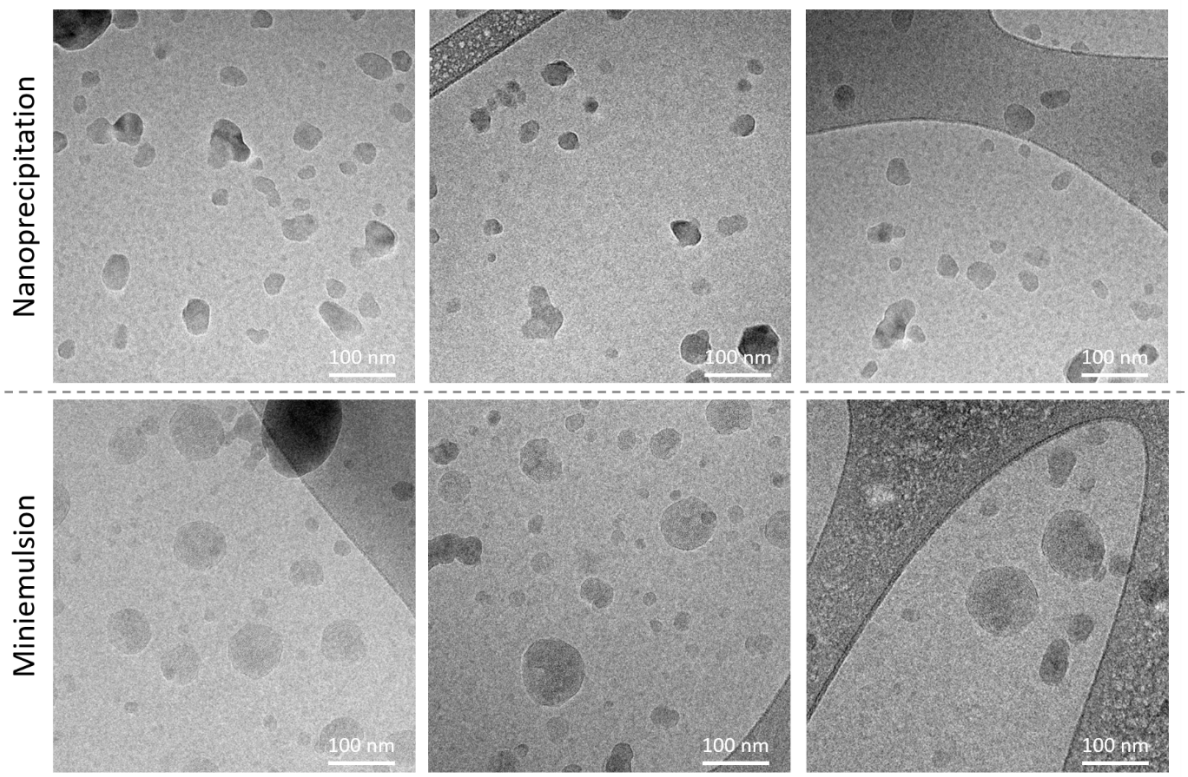

Figure S3. Cryo-TEM images of PTQ10:Y6 nanoparticles prepared through nanoprecipitation or miniemulsion, stabilised by SDS.

Supplementary note 2:

Interfacial energy between PTQ10 and Y6 can be calculated following the equation:

$$\gamma_{PTQ10/Y6} = \left[\left(\gamma_{PTQ10}^{d}\right)^{1/2} - \left(\gamma_{Y6}^{d}\right)^{1/2}\right]^2 + \left[\left(\gamma_{PTQ10}^{p}\right)^{1/2} - \left(\gamma_{Y6}^{p}\right)^{1/2}\right]^2 \quad 4$$

$$\gamma_{PTQ10/Y6} = \left[(21.2)^{1/2} - (19.2)^{1/2}\right]^2 + \left[(2.0)^{1/2} - (8.0)^{1/2}\right]^2 = 2.05 \text{ mN/m}$$

And surface tension between one material and the dispersive medium following the equation:

$$\gamma_{S/Liq} = \gamma_S - \gamma_{Liq} \cdot \cos(\theta_{S/L}) \quad (2)$$ [5,6]

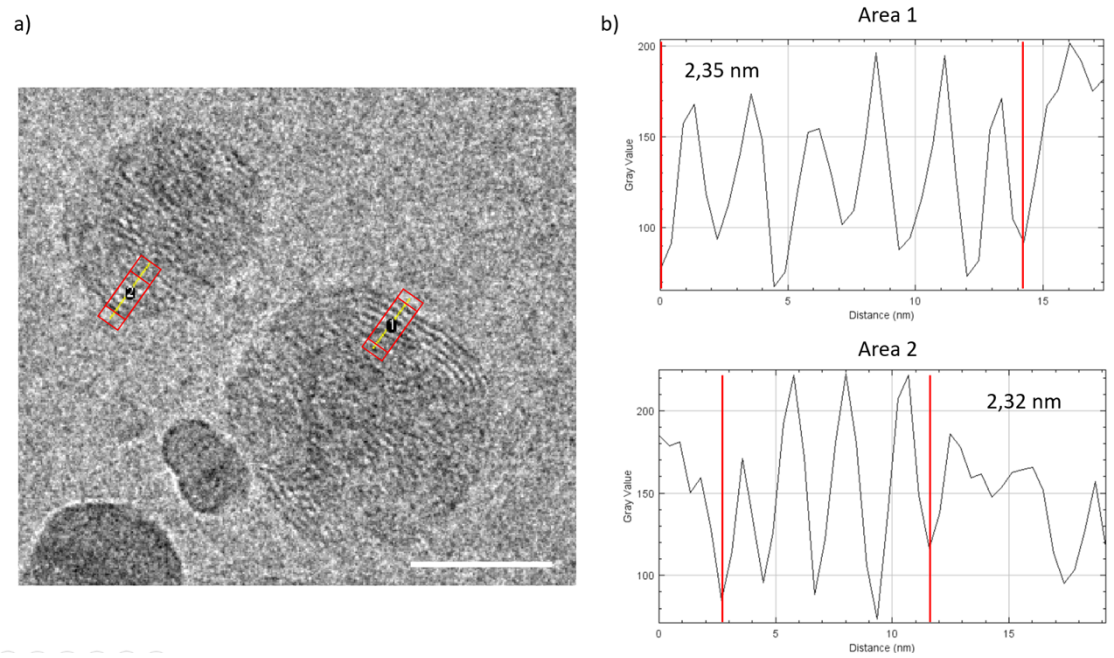

Figure S4. (a) Cryo-TEM image of PTQ10:Y6 NPs prepared by miniemulsion with crystalline areas of Y6 selected and (b) corresponding profile of periodic spacing.

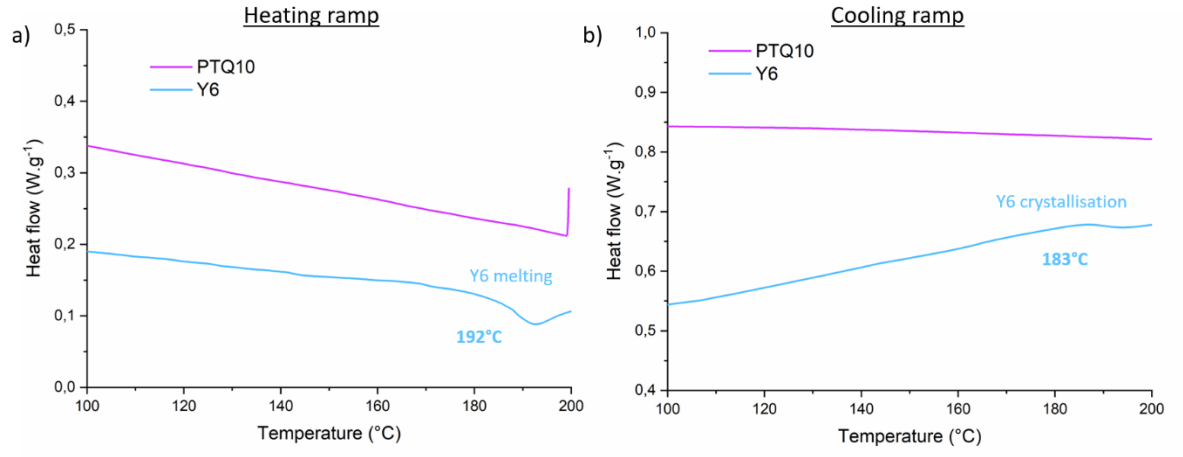

Figure S5. Differential Scanning Calorimetry thermograms upon (a) heating and (b) cooling ramps of PTQ10 and Y6 casted from chloroform. All DSC experiments were performed under nitrogen at 20°C/min.

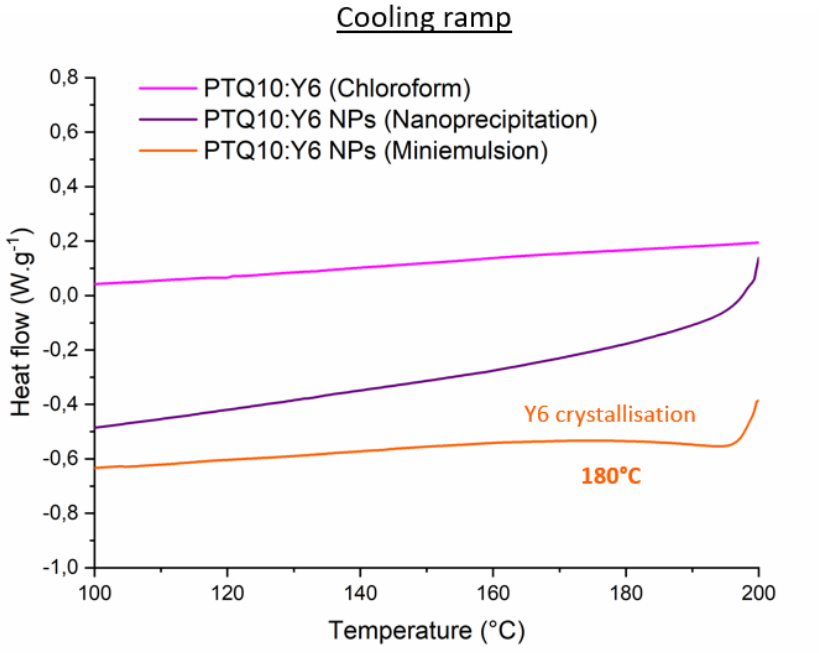

Figure S6. Differential Scanning Calorimetry thermograms upon (cooling ramps of PTQ10:Y6 casted from chloroform and PTQ10:Y6 NPs prepared by nanoprecipitation or miniemulsion. All DSC experiments were performed under nitrogen at 20°C/min.

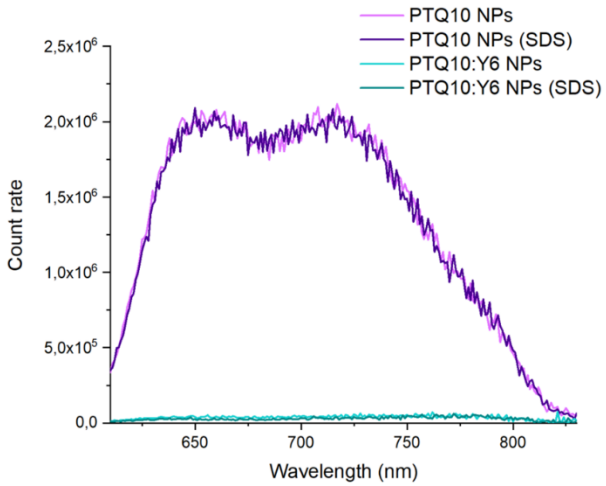

Figure S7. Emission spectra of PTQ10 and PTQ10:Y6 nanoparticles prepared by nanoprecipitation with and without SDS (excitation at 560 nm).

Supplementary note 3:

In a TAS experiment, a pump pulse populates the excited states, while an attenuated and broadband pulse probes the spectral features of the photogenerated species in a time-resolved manner. When the differential spectrum is reported in transmission units (ΔT/T), positive signals are due either to the photoinduced bleaching of the ground state (photobleaching, PB) that leads to an increase of the probe

transmission, or to a perceived enhancement of the transmission owing to the emission of a stimulated photon (stimulated emission, SE). Conversely, a negative signal is related to a decreased probe transmission due to excited state absorption (ESA).[7]

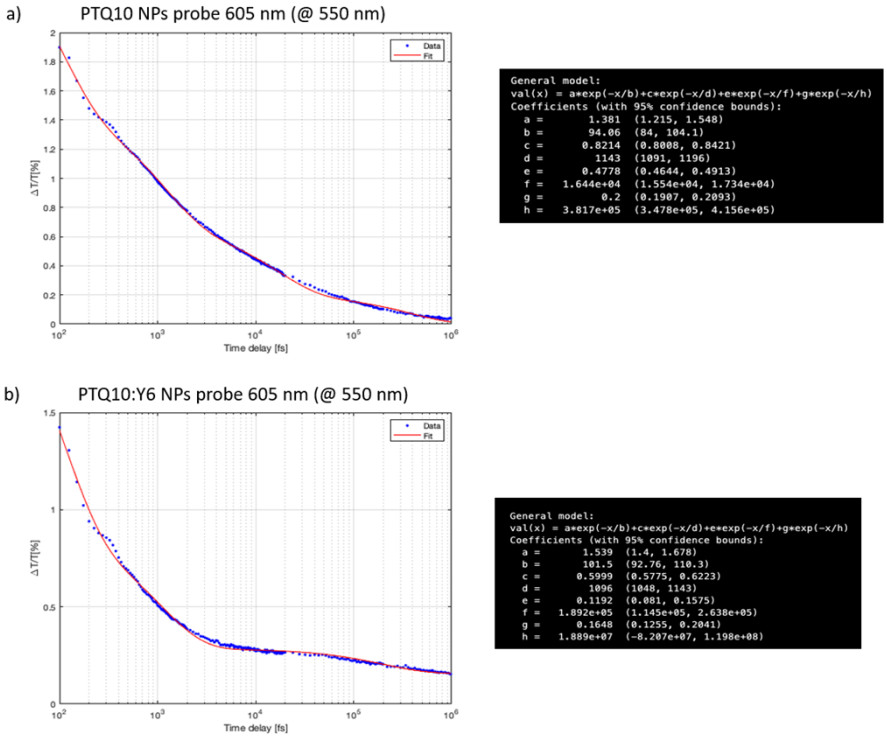

Figure S8. Fitting of transient absorption decay dynamics for (a) PTQ10 and (b) PTQ10:Y6 nanoparticles pumped at 550 nm and probed at 605 nm. Corresponding values of the fit are displayed on the right of each graph.

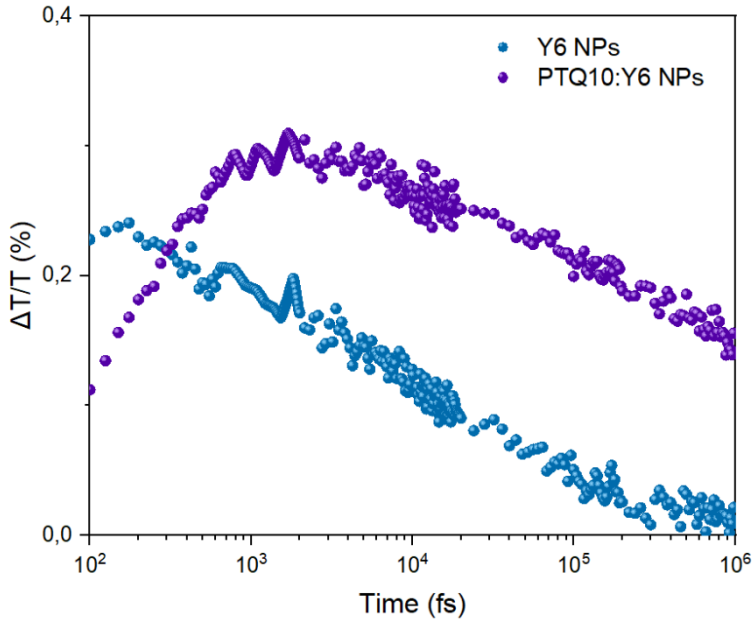

Figure S9. Comparison of transient absorption decay dynamics for Y6 and PTQ10:Y6 nanoparticles pumped at 550 nm and probed at 850 nm.

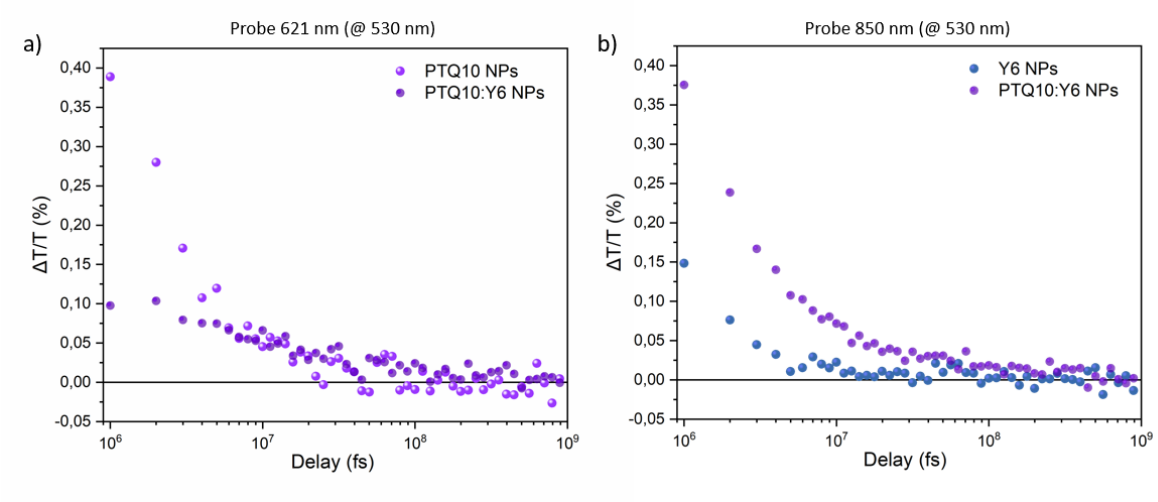

Figure S10. Comparison of transient absorption decay dynamics using picosecond laser for PTQ10, Y6 and PTQ10:Y6 nanoparticles pumped at 530 nm and probed at (a) 621 nm and (b) 850 nm.

a) PTQ10 NPs probe 621 nm (@ 530 nm)

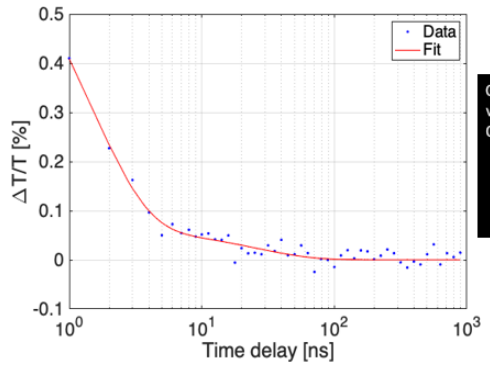


```
General model:
val(x) = a*exp(-x/tau1)+c*exp(-x/tau2)
Coefficients (with 95% confidence bounds):
  a =       0.6906  (0.5711, 0.81)
  c =      0.06514  (0.03842, 0.09186)
  tau1 =         1.45  (1.125, 1.775)
  tau2 =        25.54  (9.488, 41.59)
```

b) PTQ10:Y6 NPs probe 621 nm (@ 530 nm)

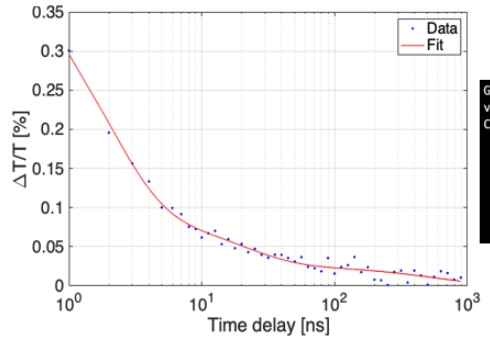


```
General model:
val(x) = a*exp(-x/tau1)+b*exp(-x/tau2)+c*exp(-x/tau3)
Coefficients (with 95% confidence bounds):
  a =      0.4989  (0.4305, 0.5672)
  b =      0.1393  (0.09337, 0.1853)
  c =     0.03044  (0.0233, 0.03759)
  tau1 =       1.237  (0.9176, 1.557)
  tau2 =        8.02  (5.198, 10.84)
  tau3 =       251.2  (132.1, 370.3)
```

c) PTQ10:Y6 NPs probe 850 nm (@ 530 nm)

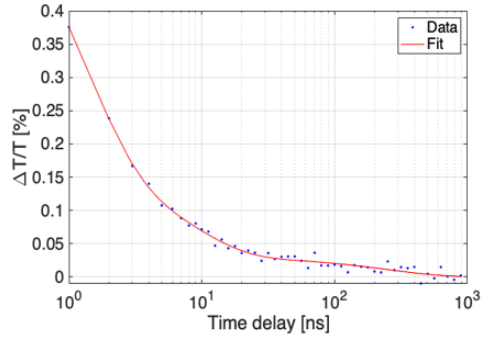


```
General model:
val(x) = a*exp(-x/tau1)+b*exp(-x/tau2)+c*exp(-x/tau3)
Coefficients (with 95% confidence bounds):
  a =       0.347  (0.3042, 0.3898)
  b =     0.07247  (0.05088, 0.09406)
  c =     0.02684  (0.01849, 0.03518)
  tau1 =       1.825  (1.418, 2.231)
  tau2 =       18.95  (9.214, 28.69)
  tau3 =       591.3  (171.5, 1011)
```

Figure S11. Fitting of transient absorption decay dynamics for (a) PTQ10 and (b, c) PTQ10:Y6 nanoparticles pumped at 530 nm and probed at (b) 621 nm and (c) 850 nm. Corresponding values of the fit are displayed on the right of each graph.

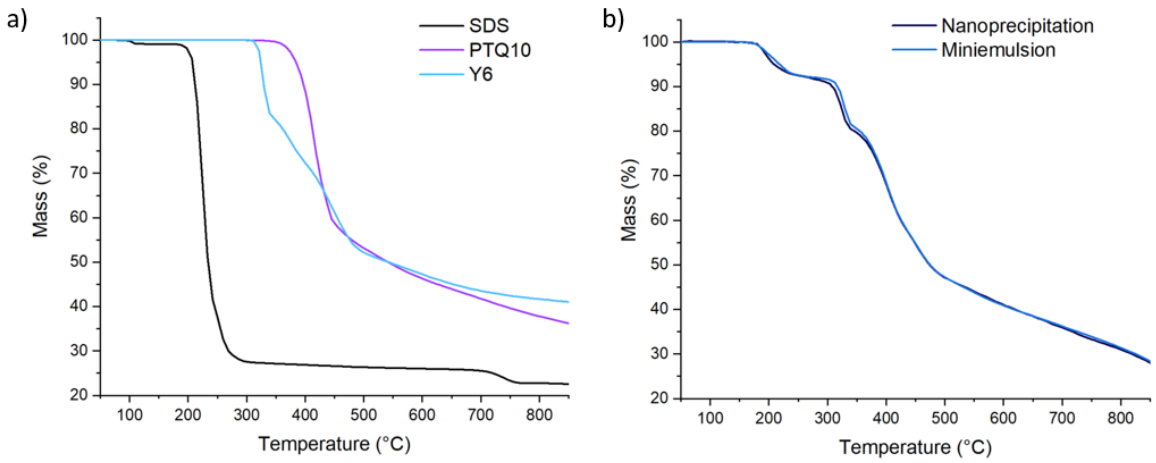

Figure S12. Thermogravimetry analysis (a) raw materials (b) PTQ10:Y6 nanoparticles stabilised by SDS prepared through nanoprecipitation and miniemulsion. Analysis conducted under nitrogen atmosphere with a heating ramp of 10°C/min.

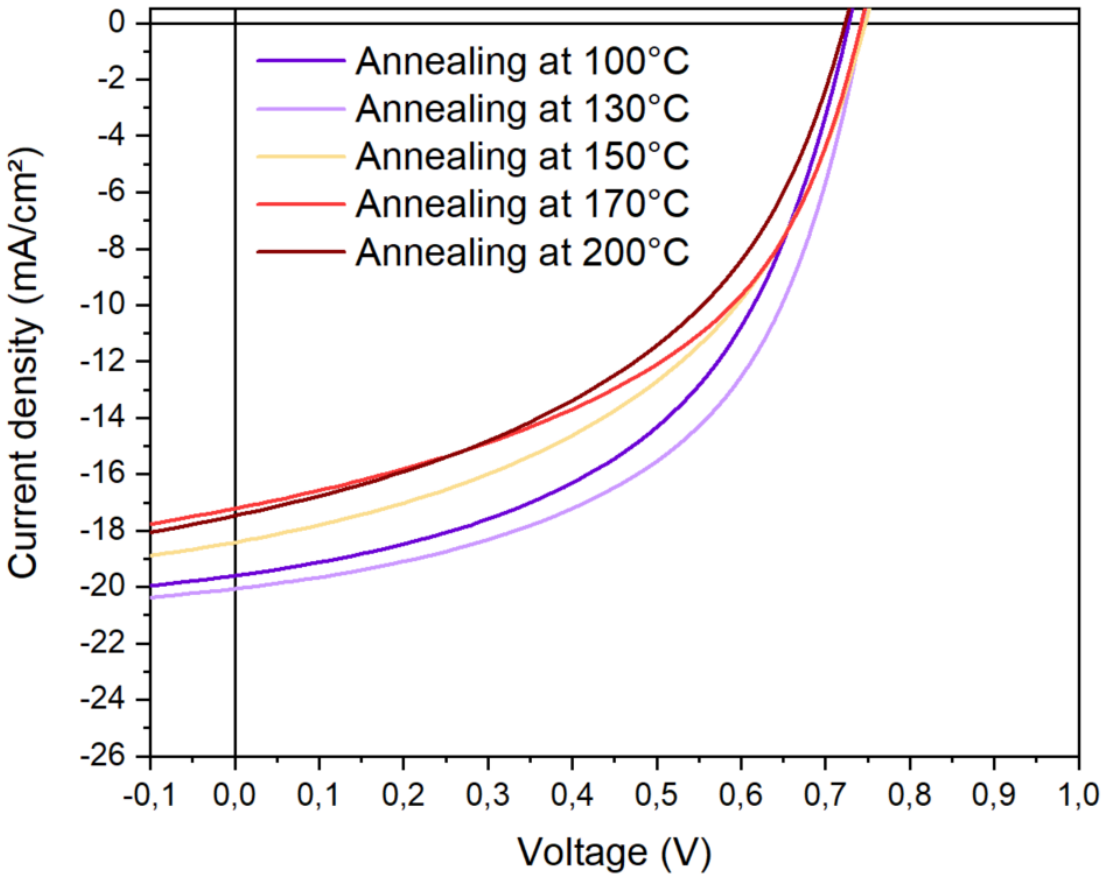

Figure S13. J-V curves of PTQ10:Y6 devices processed from aqueous dispersions of s-NPs at different annealing temperatures. Thermal treatments were performed for 2 minutes.

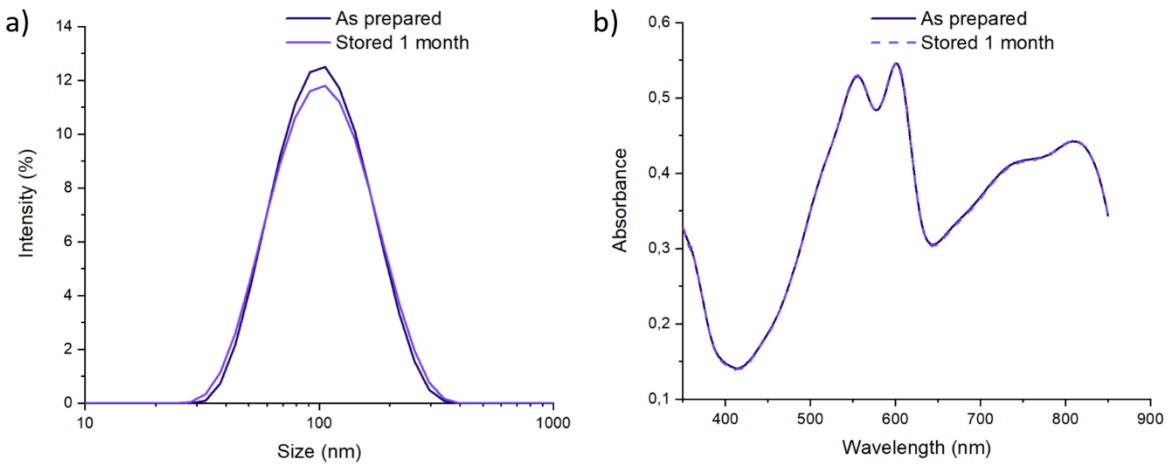

Figure S14. Evolution of (a) dispersions size distribution by DLS; (b) UV-visible absorption spectra. Nanoparticles prepared by nanoprecipitation were washed 5 times (to remove surfactant excess), concentrated to 50 mg/mL, and stored for one month in ambient atmosphere and protected from the light. No visible aggregation appears on DLS and UV-visible analysis.

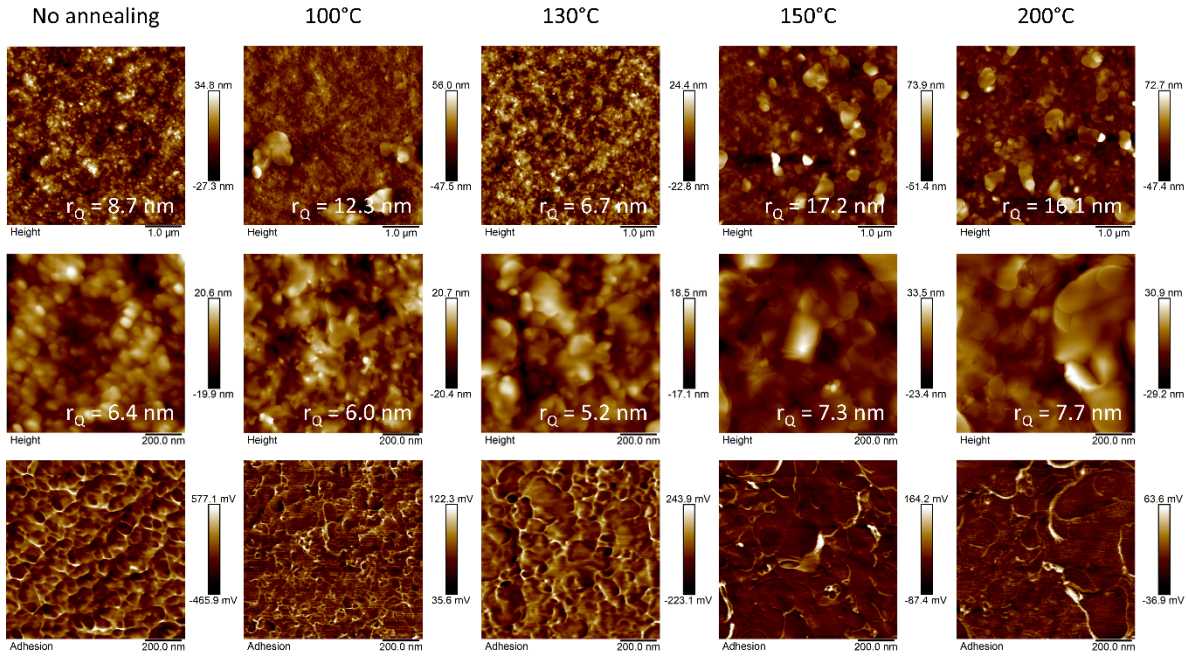

Figure S15. Evolution of film morphology upon annealing 2 minutes and various annealing temperatures for PTQ10:Y6 films processed through nanoprecipitation, according to AFM height and adhesion profiles. The film roughness r_Q is presented for each condition.

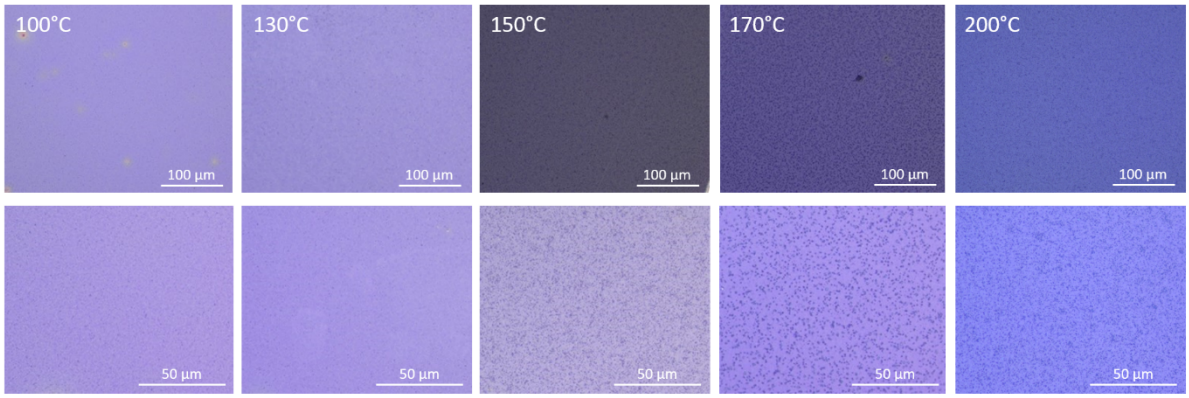

Figure S16. Optical microscopy images of PTQ10:Y6 films processed from aqueous dispersions (nanoprecipitation) at different annealing temperatures for 2 minutes.

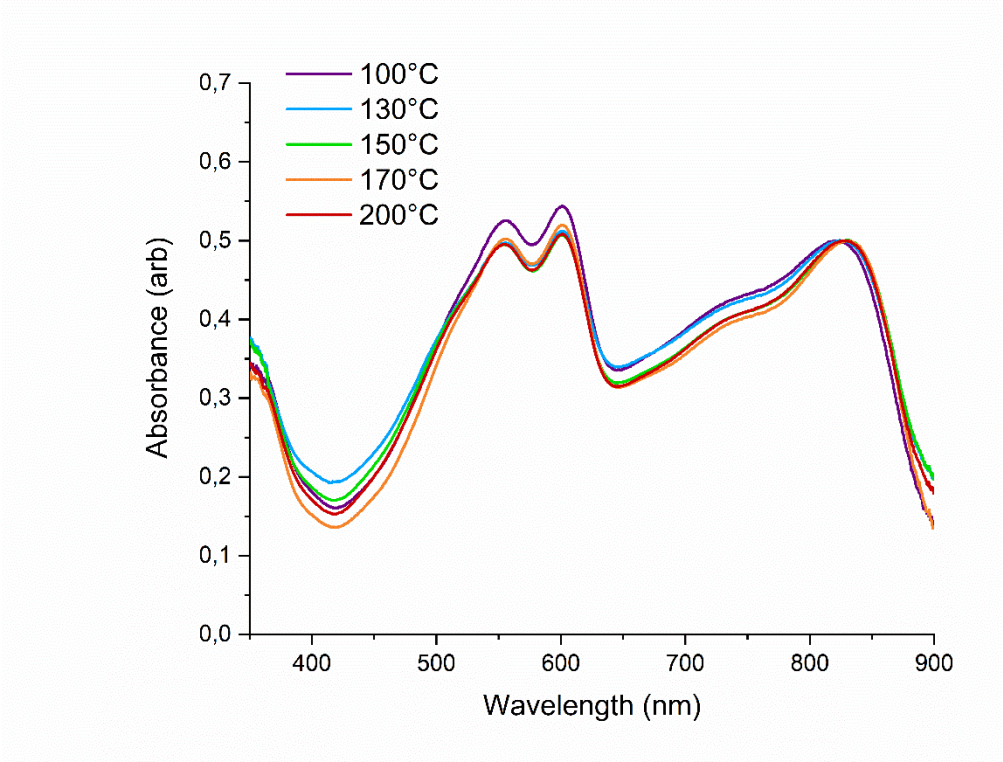

Figure S17. Visible absorption spectra of PTQ10:Y6 Nps films at different annealing temperature for 2 minutes (under nitrogen). Intensity normalised at 0.5 for the higher contribution of Y6 peak in each cases.

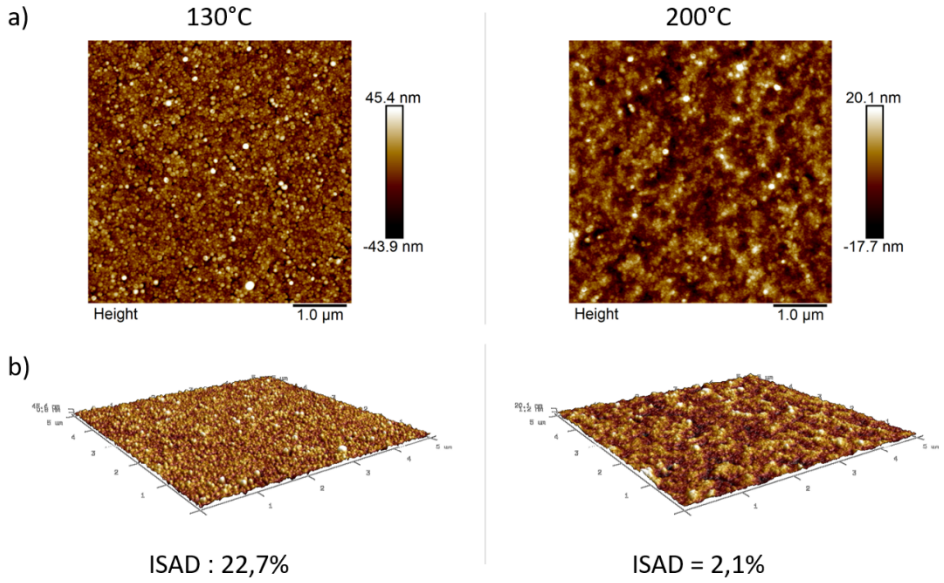

Figure S18. (a) Evolution of film morphology upon annealing for PTQ10:Y6 films processed through miniemulsion, according to AFM height profiles. (b) 3D height profiles and corresponding ISAD (Image Surface Area Difference): Projected surface/scan surface.

Supplementary tables

*Table S1. Evolution of contact angle, surface tensions and interfacial ratios depending on the choice of dispersant for PTQ10 and Y6 materials. *approximated from the average of surface tensions: water/THF and water/SDS.*

	PTQ10 contact angle (°)	Y6 contact angle (°)	γ_{dis} (mN/m)	$\gamma_{PTQ10/dis}$ (mN/m)	$\gamma_{Y6/dis}$ (mN/m)	$\gamma_{PTQ10/dis}$ /$\gamma_{PTQ10:Y6}$	$\gamma_{Y6/dis}$ /$\gamma_{PTQ10:Y6}$
Water	103.3	90.9	72.8[5]	39.4	28.3	19.5	13.8
Water/THF (8:1)	85.1	79.6	44.2[8]	19.3	19.2	9.4	9.4
Water + SDS (3 mg/mL)	66.0	62.0	33.0[5,9]	9.8	11.7	4.8	5.7
Water/THF (8:1) + SDS (3 mg/mL)	64.9	58.2	38.6*	6.8	5.5	2.7	3.3

Table S2. Influence of thickness for PTQ10:Y6 NP-based active layers (nanoprecipitation) after annealing at 130°C for 2 minutes. Average values and standard deviations calculated from at least 6 devices.

Solvent	Thickness (nm)	Jsc (mA/cm²)	Voc (mV)	FF (%)	PCE
Water (SDS)	100	19.4 ± 0.3	710 ± 31	53 ± 4	7.25% (8.10%)
	140	**21.0 ± 0.7**	**719 ± 15**	**51 ± 2**	**7.73% (8.52%)**
	180	19.1 ± 1.0	732 ± 9	51 ± 2	7.16% (7.87%)

Table S3. Influence of thermal treatment time over the performances of nanoprecipitation-based PTQ10:Y6 nanoparticles (stabilised by SDS) for annealing at 130°C. Average values and standard deviations calculated from at least 6 devices.

Solvent	Annealing time	Jsc (mA/cm²)	Voc (mV)	FF (%)	PCE
Water (SDS)	2 min	21.0 ± 0.7	719 ± 15	51 ± 2	7.73% (8.52%)
	5 min	**20.6 ± 0.3**	**726 ± 11**	**54 ± 2**	**7.99% (8.57%)**
	10 min	21.2 ± 0.3	702 ± 19	50 ± 4	7.46% (8.92%)

Table S4. Influence of time between filtration and processing over the performances of nanoprecipitation-based PTQ10:Y6 nanoparticles (stabilised by SDS). Annealing was performed at 130°C for 5 minutes under nitrogen atmosphere prior to electrode deposition. Active layer thickness of 140 nm. Average values and standard deviations calculated from at least 6 devices.

Solvent	Filtration time	Jsc (mA/cm²)	Voc (mV)	FF (%)	PCE
Water (SDS)	1 week	20.8 ± 0.3	722 ± 4	51 ± 1	7.60% (7.84%)
	1 day	20.6 ± 0.3	723 ± 11	54 ± 2	7.99% (8.57%)
	10 minutes	**22.1 ± 0.5**	**746 ± 7**	**59 ± 1**	**9.74% (10.14%)**

Table S5. Evolution of photovoltaic parameters of PTQ10:Y6 h-NPs devices prepared by miniemulsion for different annealing temperature. Annealing was performed under nitrogen atmosphere prior to electrode deposition. Active layer thickness of 140 nm. Average values and standard deviations calculated from at least 4 devices.

Solvent	Technique	Annealing Temperature (°C)	Jsc (mA/cm²)	Voc (mV)	FF (%)	PCE
Water (SDS)	Miniemulsion (ME)	100	9.3 ± 0.2	721 ± 6	46 ± 1	3.10% (3.18%)
		130	12.1 ± 0.2	718 ± 7	48 ± 2	4.20% (4.41%)
		150	15.3 ± 0.3	686 ± 49	46 ± 7	4.80% (5.93%)
		170	16.1 ± 0.3	721 ± 5	52 ±7	5.91% (6.57%)
		200	**18.0 ± 0.2**	**695 ± 5**	**59 ± 2**	**7.32% (7.71%)**

Table S6. Photovoltaic performances of water-based devices in the literature (updated September 2023).

Year	System	Technique	Cell surface (mm²)	Annealing	Surfactant	Voc (V)	Jsc ($mA.cm^{-2}$)	FF (%)	PCE (%)	Ref
2011	P1:$PC_{61}BM$	ME	400	-	SDS	0.24	1.1	27.5	0.07	[10]

	PSBTBT:$PC_{61}BM$		400	-		0.47	3.99	29.3	0.55	
	P3:$PC_{61}BM$		400	-		0.54	0.92	30.8	0.15	
2012	P3HT:$PC_{61}BM$	ME	-	140°C (-)	SDS	0.45	1.95	33.1	0.29	[11]
2013	P3HT:$PC_{61}BM$	ME	5	110°C (4 min)	SDS	0.52	5.45	47.0	1.31	[12]
	P3HT:ICBA	ME	5	150°C (15 min)	SDS	0.79	5.57	57.0	2.50	[13]
2014	PDPPTNT:$PC_{71}BM$	ME	3.9	130°C (10 min)	SDS	0.76	6.09	43.0	1.99	[14]
	P3HT:$PC_{61}BM$	ME	6	150°C (-)	SDS	0.51	6.38	66.2	2.15[1]	[15]
			-	140°C (4 min)		0.54	4.73	47.0	1.20	[16]
			6	150°C (-)		0.52	6.38	67.9	2.15[1]	[17]
2015	PSBTBT:$PC_{61}BM$	ME	25	140°C (2 min)	SDS	0.62	6.20	33	1.3	[18]
	P3HT:$PC_{61}BM$		5	110°C (4 min)	SDS	0.52	4.60	42.0	1.00	[19]
			12	80°C (60 min)		0.47	4.89	50.5	1.16	[20]
	P(TBT-DPP):ICBA	ME	4	150°C (20 min)	SDS	0.44	12.73	47.0	2.63	[21]
2016	TQ1:$PC_{71}BM$	ME	-	140°C (5 min)	SDS	0.70	10.06	36.0	2.54	[22]
2017	PBDTTPD:$PC_{71}BM$	ME	3	180°C (20 min)	SDS	0.86	9.99	44.0	3.80	[23]
	PDPP5T:$PC_{71}BM$	ME	16	110°C (10 min) + 140°C (10 min)	SDS	0.54	9.34	47.0	2.36	[24]
	PCDTBT:$PC_{71}BM$	ME	30	180°C (4 min)	SDS	0.57	8.69	38.0	1.90	[25]
		ME	10	140°C (4 min)	SDS	0.61	3.79	30.7	0.70	[26]
2018	P3HT:ICxA	ME	3.8	110°C (10 min)	SDS	0.59	3.81	39	0.87	[27]
			3.8	110°C (10 min)		0.50	3.64	51	0.73	[28]
	PCDTBT:$PC_{71}BM$	NPt	10	160°C (4 min)	—	0.48	1.65	29.0	0.19	[29]
	PDPP5T-2:$PC_{71}BM$	ME	10.4	150°C (10 min)	SDS	0.54	11.59	49.0	3.38	[30]
	PTNT:$PC_{71}BM$	ME	10	160°C (5 min) + post TT	SDS	0.89	4.73	39.0	1.65	[31]
	P3HT:o-IDTBR	NPt	10.4	150°C (10 min)	F127	0.76	10.36	62.9	4.95	[32]
		ME	10.4	150°C (10 min)	SDS	0.75	7.45	45.2	2.54	
	PCE10:o-IDTBR	NPt	10.4	150°C (10 min)	F127	0.97	12.01	42.4	4.94	
		ME	10.4	150°C (10 min)	SDS	0.97	9.20	40.7	3.61	
	PBQ-QF:o-IDTBR	NPt	10.4	150°C (10 min)	F127	0.95	13.09	47.9	5.96	
		ME	10.4	150°C (10 min)	SDS	0.92	9.79	38.3	3.45	
	PBQ-QF:ITIC	NPt	10.4	150°C (10 min)	F127	0.85	14.87	52.7	6.97	
		ME	10.4	150°C (10 min)	SDS	0.84	10.31	46.0	3.98	
2019	P3HT:ICxA	ME	1950	-	SDS	0.58	5.91	0.44	1.51	[33]
	P3HT:$PC_{61}BM$	ME	4	110°C (4 min)	SDS	0.38	7.1	44.0	1.20	[34]
2021	BCP:$PC_{61}BM$	ME	2	90°C (20 min)	BCP	0.64	10.6	36.7	2.49	[35]
2022	P3HT:$PC_{61}BM$	ME	4	110°C (5 min)	SDS	0.42	5.3	43	1.24	[36]
			4	110°C (5 min)	TEBS	0.46	6.4	48	1.55	
	PM6:BTP-eC9	NPt	0.06	100°C (10 min)	F127	0.72	18.2	65	8.52	[37]
			0.06	100°C (10 min)		0.77	20.4	68	10.70[2]	
2023	PTB7:$PC_{71}BM$	ME	32	140°C (10 min)	SDS	0.69	7.08	35	2.17	[38]

			32	140°C (10 min)		0.74	7.93	49	3.35[3]	
	PTB7-Th:$PC_{71}BM$	ME	32	140°C (10 min)	SDS	0.72	8.85	36	3.16	
			32	140°C (10 min)		0.74	12.6	46	5.11[3]	
	PTQ10:Y6	ME	10.5	200°C (2 min)	SDS	0.72	21.1	62	9.98	[39]
This Work	**PTQ10:Y6**	**ME**	**10.5**	**200°C (2 min)**	**SDS**	**0.69**	**18.0**	**59**	**7.71**	**-**
		NPt	**10.5**	**130°C (5 min)**	**SDS**	**0.75**	**22.1**	**59**	**10.14**	

[1]: $PC_{61}BM$ layer casted from DCB solution

[2]: DIO used as additive

[3]: ME process modified to achieve Janus nanoparticles (instead of core-shell)

1 D. Kroh, F. Eller, K. Schötz, S. Wedler, L. Perdigón-Toro, G. Freychet, Q. Wei, M. Dörr, D. Jones, Y. Zou, E. M. Herzig, D. Neher and A. Köhler, *Adv. Funct. Mater.*, 2022, **32**, 2205711.
2 G. Kupgan, X. K. Chen and J. L. Brédas, *Mater. Today Adv.*, 2021, **11**, 100154.
3 L. Perdigón-Toro, L. Q. Phuong, F. Eller, G. Freychet, E. Saglamkaya, J. I. Khan, Q. Wei, S. Zeiske, D. Kroh, S. Wedler, A. Köhler, A. Armin, F. Laquai, E. M. Herzig, Y. Zou, S. Shoaee and D. Neher, *Adv. Energy Mater.*, 2022, **12**, 2103422.
4 F.-C. Wu, C.-C. Yang, P.-T. Tseng, W.-Y. Chou and H.-L. Cheng, eds. C. E. Tabor, F. Kajzar, T. Kaino and Y. Koike, San Francisco, California, United States, 2017, p. 101011D.
5 A. R. Harikrishnan, S. K. Das, P. K. Agnihotri and P. Dhar, *J. Appl. Phys.*, 2017, **122**, 054301.
6 Y. Wang, B.-H. Guo, X. Wan, J. Xu, X. Wang and Y.-P. Zhang, *Polymer*, 2009, **50**, 3361–3369.
7 G. M. Paternò, L. Moretti, A. J. Barker, Q. Chen, K. Müllen, A. Narita, G. Cerullo, F. Scotognella and G. Lanzani, *Adv. Funct. Mater.*, 2019, **29**, 1805249.
8 J. Shen, J. Wu, M. Wang, P. Dong, J. Xu, X. Li, X. Zhang, J. Yuan, X. Wang, M. Ye, R. Vajtai, J. Lou and P. M. Ajayan, *Small*, 2016, **12**, 2741–2749.
9 F. Hernáinz-Bermúdez de Castro, A. Gálvez-Borrego and M. Calero-de Hoces, *J. Chem. Eng. Data*, 1998, **43**, 717–718.
10 T. R. Andersen, T. T. Larsen-Olsen, B. Andreasen, A. P. L. Böttiger, J. E. Carlé, M. Helgesen, E. Bundgaard, K. Norrman, J. W. Andreasen, M. Jørgensen and F. C. Krebs, *ACS Nano*, 2011, **5**, 4188–4196.
11 T. T. Larsen-Olsen, B. Andreasen, T. R. Andersen, A. P. L. Böttiger, E. Bundgaard, K. Norrman, J. W. Andreasen, M. Jørgensen and F. C. Krebs, *Sol. Energy Mater. Sol. Cells*, 2012, **97**, 22–27.
12 S. Ulum, N. Holmes, D. Darwis, K. Burke, A. L. David Kilcoyne, X. Zhou, W. Belcher and P. Dastoor, *Sol. Energy Mater. Sol. Cells*, 2013, **110**, 43–48.
13 S. Ulum, N. Holmes, M. Barr, A. L. D. Kilcoyne, B. B. Gong, X. Zhou, W. Belcher and P. Dastoor, *Nano Energy*, 2013, **2**, 897–905.
14 B. Vaughan, E. L. Williams, N. P. Holmes, P. Sonar, A. Dodabalapur, P. C. Dastoor and W. J. Belcher, *Phys. Chem. Chem. Phys.*, 2014, **16**, 2647.
15 T. S. Gehan, M. Bag, L. A. Renna, X. Shen, D. D. Algaier, P. M. Lahti, T. P. Russell and D. Venkataraman, *Nano Lett.*, 2014, **14**, 5238–5243.
16 N. P. Holmes, S. Ulum, P. Sista, K. B. Burke, M. G. Wilson, M. C. Stefan, X. Zhou, P. C. Dastoor and W. J. Belcher, *Sol. Energy Mater. Sol. Cells*, 2014, **128**, 369–377.
17 M. Bag, T. S. Gehan, L. A. Renna, D. D. Algaier, P. M. Lahti and D. Venkataraman, *RSC Adv.*, 2014, **4**, 45325–45331.
18 H. F. Dam, N. P. Holmes, T. R. Andersen, T. T. Larsen-Olsen, M. Barr, A. L. D. Kilcoyne, X. Zhou, P. C. Dastoor, F. C. Krebs and W. J. Belcher, *Sol. Energy Mater. Sol. Cells*, 2015, **138**, 102–108.
19 N. P. Holmes, N. Nicolaidis, K. Feron, M. Barr, K. B. Burke, M. Al-Mudhaffer, P. Sista, A. L. D. Kilcoyne, M. C. Stefan, X. Zhou, P. C. Dastoor and W. J. Belcher, *Sol. Energy Mater. Sol. Cells*, 2015, **140**, 412–421.
20 E. B. L. Pedersen, M. C. Pedersen, S. B. Simonsen, R. G. Brandt, A. P. L. Böttiger, T. R. Andersen, W. Jiang, Z. Y. Xie, F. C. Krebs, L. Arleth and J. W. Andreasen, *J. Mater. Chem. A*, 2015, **3**, 17022–17031.
21 N. A. D. Yamamoto, M. E. Payne, M. Koehler, A. Facchetti, L. S. Roman and A. C. Arias, *Sol. Energy Mater. Sol. Cells*, 2015, **141**, 171–177.
22 N. P. Holmes, M. Marks, P. Kumar, R. Kroon, M. G. Barr, N. Nicolaidis, K. Feron, A. Pivrikas, A. Fahy, A. D. de Z. Mendaza, A. L. D. Kilcoyne, C. Müller, X. Zhou, M. R. Andersson, P. C. Dastoor and W. J. Belcher, *Nano Energy*, 2016, **19**, 495–510.
23 L. D'Olieslaeger, G. Pirotte, I. Cardinaletti, J. D'Haen, J. Manca, D. Vanderzande, W. Maes and A. Ethirajan, *Org. Electron.*, 2017, **42**, 42–46.
24 F. J. M. Colberts, M. M. Wienk and R. A. J. Janssen, *ACS Appl. Mater. Interfaces*, 2017, **9**, 13380–13389.
25 L. D'Olieslaeger, M. Pfannmöller, E. Fron, I. Cardinaletti, M. Van Der Auweraer, G. Van Tendeloo, S. Bals, W. Maes, D. Vanderzande, J. Manca and A. Ethirajan, *Sol. Energy Mater. Sol. Cells*, 2017, **159**, 179–188.

26 L. Parrenin, G. Laurans, E. Pavlopoulou, G. Fleury, G. Pecastaings, C. Brochon, L. Vignau, G. Hadziioannou and E. Cloutet, *Langmuir*, 2017, **33**, 1507–1515.
27 F. Almyahi, T. R. Andersen, N. Cooling, N. P. Holmes, A. Fahy, M. G. Barr, D. Kilcoyne, W. Belcher and P. C. Dastoor, *Org. Electron.*, 2018, **52**, 71–78.
28 F. Almyahi, T. R. Andersen, N. A. Cooling, N. P. Holmes, M. J. Griffith, K. Feron, X. Zhou, W. J. Belcher and P. C. Dastoor, *Beilstein J. Nanotechnol.*, 2018, **9**, 649–659.
29 G. Prunet, L. Parrenin, E. Pavlopoulou, G. Pecastaings, C. Brochon, G. Hadziioannou and E. Cloutet, *Macromol. Rapid Commun.*, 2018, **39**, 1700504.
30 C. Xie, A. Classen, A. Späth, X. Tang, J. Min, M. Meyer, C. Zhang, N. Li, A. Osvet, R. H. Fink and C. J. Brabec, *Adv. Energy Mater.*, 2018, **8**, 1702857.
31 X. Pan, A. Sharma, D. Gedefaw, R. Kroon, A. Diaz de Zerio, N. P. Holmes, A. L. D. Kilcoyne, M. G. Barr, A. Fahy, M. Marks, X. Zhou, W. Belcher, P. C. Dastoor and M. R. Andersson, *Org. Electron.*, 2018, **59**, 432–440.
32 C. Xie, T. Heumüller, W. Gruber, X. Tang, A. Classen, I. Schuldes, M. Bidwell, A. Späth, R. H. Fink, T. Unruh, I. McCulloch, N. Li and C. J. Brabec, *Nat. Commun.*, 2018, **9**, 5335.
33 F. Almyahi, T. R. Andersen, A. Fahy, M. Dickinson, K. Feron, W. J. Belcher and P. C. Dastoor, *J. Mater. Chem. A*, 2019, **7**, 9202–9214.
34 M. Marks, N. P. Holmes, A. Sharma, X. Pan, R. Chowdhury, M. G. Barr, C. Fenn, M. J. Griffith, K. Feron, A. L. D. Kilcoyne, D. A. Lewis, M. R. Andersson, W. J. Belcher and P. C. Dastoor, *Phys. Chem. Chem. Phys.*, 2019, **21**, 5705–5715.
35 A. M. Ferretti, M. Diterlizzi, W. Porzio, U. Giovanella, L. Ganzer, T. Virgili, V. Vohra, E. Arias, I. Moggio, G. Scavia, S. Destri and S. Zappia, *Nanomaterials*, 2021, **12**, 84.
36 R. Chowdhury, N. P. Holmes, N. Cooling, W. J. Belcher, P. C. Dastoor and X. Zhou, *ACS Omega*, 2022, **7**, 9212–9220.
37 C. Xie, S. Liang, G. Zhang and S. Li, *Polymers*, 2022, **14**, 4229.
38 Y. Du, Y. Wang, V. Shamraienko, K. Pöschel and A. Synytska, *Small*, 2023, 2206907.
39 H. Laval, A. Holmes, M. A. Marcus, B. Watts, G. Bonfante, M. Schmutz, E. Deniau, R. Szymanski, C. Lartigau-Dagron, X. Xu, J. M. Cairney, K. Hirakawa, F. Awai, T. Kubo, G. Wantz, A. Bousquet, N. P. Holmes and S. Chambon, *Adv. Energy Mater.*, 2023, 2300249.